Appl. Phys. B (2016) 122:100
DOI 10.1007/s00340-016-6378-z

Applied Physics B
Lasers and Optics

Detection of methyl mercaptan with a 3393-nm distributed feedback interband cascade laser

Zhenhui Du[1] · Weimeng Zhen[1] · Zheyuan Zhang[1] · Jinyi Li[2] · Nan Gao[3]

Received: 3 July 2015 / Accepted: 1 March 2016 / Published online: 12 April 2016

Abstract Attention has been focused recently on the harmful effects and malodor of methyl mercaptan (CH_3SH), so it is desired to detect CH_3SH in situ, sensitively, and selectively. We detected methyl mercaptan via tunable laser absorption spectroscopy (TLAS) with a room-temperature distributed feedback interband cascade laser emitting around 3393 nm and a hollow waveguide gas cell with 5 m length. The fundamental characteristic fingerprint absorptions of CH_3SH from 3260 to 3400 nm were examined, and the spectral line 3393.584 nm (corresponding to the ν_2 C–H symmetric stretch) was determined to be the optimum for CH_3SH detection. The response characteristics of the TLAS system were established by implementing a set of CH_3SH concentration gradient experiments with wavelength-scanned direct absorption spectroscopy. The results show that CH_3SH TLAS spectra are in excellent agreement with spectra from the Pacific Northwest National Laboratory database; the TLAS response linearity is 0.987, and the detection limit is as low as 25 ppbv (parts per billion by volume, 10^{-9}) with integrated time 1.84 s, corresponding to an absorbance of 1.34×10^{-4} (near the theoretical detection limit). Overall, the TLAS system is a robust method for CH_3SH monitoring of industrial waste gas emissions.

✉ Zhenhui Du
duzhenhui@tju.edu.cn

[1] State Key Laboratory of Precision Measuring Technology and Instruments, Tianjin University, No. 92, Weijin Road, Tianjin, China

[2] School of Electrical Engineering and Automation, Tianjin Polytechnic University, No. 63, Chenglin Road, Tianjin, China

[3] School of Mechanical Engineering, Hebei University of Technology, No. 8, Guangrong Road, Tianjin, China

1 Introduction

Methyl mercaptan (CH_3SH, methanethiol) is a colorless, flammable gas with an extremely repulsive smell and is produced by both natural and industrial sources. Natural emission derives from biological degradation products and is a metabolic by-product [1]. Industrial sources include waste gases from pulp and paper production [2], landfill facilities [3], pit latrines [4], and pig farming [5]. It has a low odor threshold of 1.6 ppbv (parts per billion by volume, 10^{-9}) [6] and is highly toxic at high concentrations because it harms to the central nervous system. There are many requirements for monitoring methyl mercaptan, for example, high-sensitivity detection of exhaled CH_3SH with ppm level for rapid noninvasive diagnosis of stomach and periodontal diseases [7]; ultra-sensitivity detection of CH_3SH with ppt (parts per trillion) level for interstellar life detection [8]; and continuous or real-time monitoring of CH_3SH from ppbv to tens of ppmv levels for environmental and ecological monitoring [9].

Common methods for detecting CH_3SH include combined gas chromatography and mass spectroscopy (GC–MS) [10–12], gas sensors [13–19], and infrared absorption spectroscopy [8]. GC–MS provides qualitative and quantitative analysis with high accuracy, which can reach ppbv level. However, it is time consuming and costly. Sensors such as electrochemical devices [13–15] and detector tubes [19] have low sensitivity, and the detection sensitivity of the electrochemical sensor is ppmv, which is much higher than the odor threshold of CH_3SH [13], while biosensors [16–18] have a good gas selectivity with a ppb detection level, but with a short lifetimes. Vance et al. [8] characterize CH_3SH absorption with a carbon isotope laser spectrometer and recommend using a 3.27-μm infrared tunable

diode laser spectrometer for in situ detection of bio-signatures for Earth-based and extraterrestrial exploration. For atmospheric CH_3SH detection, however, the spectral line absorption at 3.27 μm is subject to significant interference, primarily due to methane absorption.

Tunable laser absorption spectroscopy (TLAS) has been demonstrated to have high sensitivity and good selectivity for real-time, in situ trace gas sensing [20]. Mid-infrared (MIR) region is especially attractive for strong fundamental characteristic fingerprint absorption of many hydrocarbons. The development of commercial room-temperature single-mode mid-infrared laser has promoted high-sensitivity detection of propane [21], acetylene [22, 23], formaldehyde [24, 25], and ethane [26].

In this article, we use the Pacific Northwest National Laboratory (PNNL) [27] and high resolution transmission (HITRAN) spectroscopic databases [28] to screen CH_3SH absorption and nearby interfering atmospheric spectra to determine an optimum spectral line for CH_3SH detection. Based on the selected spectra line at 3393.584 nm, a room-temperature distributed feedback interband cascade laser (DFB-ICL) and a hollow waveguide (HWG) gas cell were used to perform wavelength-scanned direct absorption spectroscopy (DAS). A set of CH_3SH concentration experiments established the TLAS linearity to demonstrate the feasibility of CH_3SH detection in industrial applications.

2 Principle

2.1 Beer–Lambert law

The basic principle behind the TLAS technique is that the wavelength of a laser is tuned over a particular absorption line of interest and the intensity of the transmitted radiation is measured. The transmitted intensity can be related to the concentration of the species present by the Beer–Lambert law, which states that when a radiation of wavenumber (ν) passes through an absorbing medium, the intensity variation along the path of the beam is given by:

$$I(\nu) = I_0(\nu)\exp[-\alpha(\nu)L] = I_0(\nu)\exp[-\sigma(\nu)NL] \quad (1)$$

$$\alpha(\nu) = \sigma(\nu)N = S(T)\phi(\nu - \nu_0) \quad (2)$$

where $I(\nu)$ is the transmitted intensity of the radiation after it has traversed a distance L through the medium, $I_0(\nu)$ is the initial intensity of the radiation, $\alpha(\nu)$ is the absorbance of the medium, $\sigma(\nu)$ is the absorption cross section of the absorbing species, N is the number density of the absorbing species, $S(T)$ is the line strength (i.e., the total absorption per molecule) of the absorbing species at temperature T, $\phi(\nu - \nu_0)$ is the lineshape function for the particular absorption line, and ν_0 is the center frequency of the spectrum.

To detect CH_3SH with specificity and high sensitivity, the fundamental characteristic fingerprint absorptions of CH_3SH should be examined.

2.2 Selection of spectral region

The dominant infrared absorptions for CH_3SH are attributed to the fundamental C–H, S–H, C–S, and methyl vibrations. Figure 1 shows the Fourier transform infrared (FTIR) spectrum from the PNNL database of 1 ppm × m CH_3SH with 0.06 cm^{-1} resolution over the range 690–3270 cm^{-1} [27]. According to the PNNL database, we know that the strongest fundamental characteristic fingerprint absorption feature around 2948 cm^{-1} (3392.13 nm) corresponds to the C–H symmetric stretch (ν_2 band).

To monitor CH_3SH with high sensitivity, we examined the specificity of the CH_3SH absorption features from 3260 to 3400 nm (ν_1 and ν_2 bands) and those of adjacent lines of common components in an industrial atmosphere. The screening guidelines for optimum spectral lines selection are: (1) strong absorption strength, (2) large spectral separation, and (3) adequate isolation from nearby interference [29].

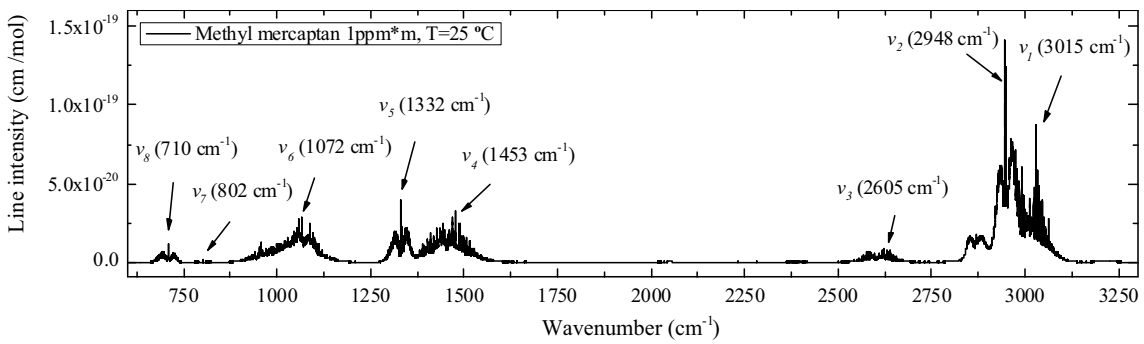

Fig. 1 Absorption spectrum of 1 ppm × m CH_3SH with 0.06 cm^{-1} resolution at 25 °C (from the PNNL database)

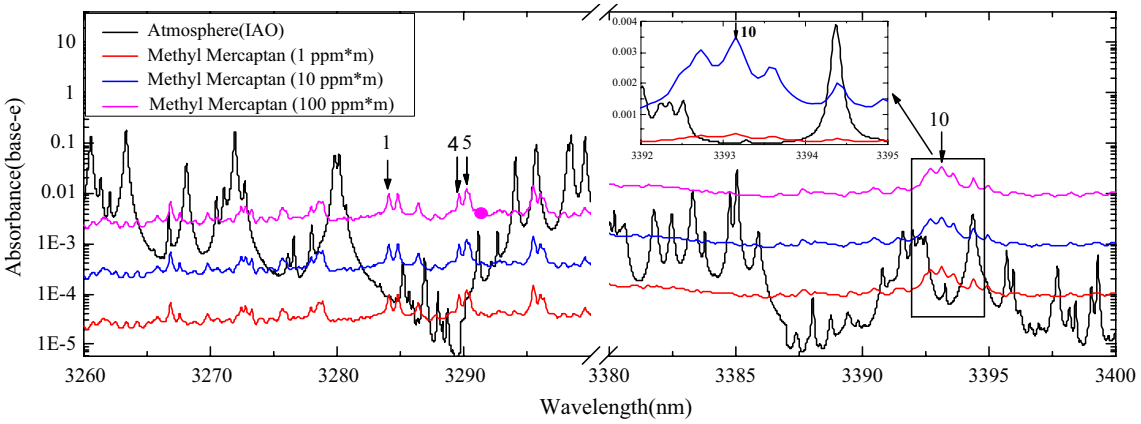

Fig. 2 Absorption spectrum of the IAO atmospheric model (from the HITRAN database) versus CH_3SH at concentrations of 100 ppm × m, 10 ppm × m and 1 ppm × m, respectively, (from the PNNL database)

Table 1 Candidate spectral lines for in situ CH_3SH sensing (with 1-m optical path length)

SN	λ (CH_3SH) (nm)	Absorbance (10 ppm CH_3SH)	λ (interference) (nm)	Absorbance (interference)	Line spacing (nm)
1	3283.997	0.000423	3283.320	0.00019	0.677
2	3284.738	0.00043	3285.163	0.0005	0.425
3	3286.353	0.000285	3286.288	0.000038	0.064
4	3289.618	0.000405	3288.664	0.000058	0.954
5	3290.146	0.000512	3291.103	0.00195	0.957
6	3344.457	0.00000615	3344.902	0.0054	0.445
7	3350.194	0.000561	3350.973	0.0106	0.780
8	3392.735	0.0013	3392.515	0.00163	0.220
9	3393.146	0.00147	3393.287	0.000205	0.142
10	3393.584	0.00107	3393.287	0.000205	0.297

SN serial number of the candidate spectral line and *line spacing* the wavelength space between CH_3SH and its nearby interference

To discuss nearby interfering absorptions by atmospheric components, we use the IAO Standard Atmosphere (V.E. Zuev Institute of Atmospheric Optics) from the HITRAN database [28]. IAO components and their abundances (mean latitude, summer, H = 0) include H_2O (1.560000 %), CO_2 (0.033300 %), O_3 (0.000002 %), N_2O (0.000028 %), CO (0.000047 %), CH_4 (0.000148 %), O_2 (20.700000 %), SO_2 (0.000008 %), NH_3 (0.000001 %), and N_2 (77.706466 %). Figure 2 shows the absorption spectra of the above IAO atmospheric model (with 1-m optical path length) and spectra for 100-, 10-, and 1-ppm × m CH_3SH. According to the Beer–Lambert law, absorbance is proportional to the concentration and the optical length. Therefore, the spectra of 10 ppm × m and 100 ppm × m derived from the spectrum of 1 ppm × m CH_3SH, which was multiplied by 10 and 100, respectively. We can conclude from Fig. 2, when the CH_3SH concentration is lower than several ppm, it is difficult to detect CH_3SH in the atmosphere, because CH_3SH absorption feature is not easily distinguishable from the interfering atmospheric absorption. However, when the CH_3SH concentration is higher than ten ppm, some absorption features are isolated from the interference and can be identified. These are indicated by vertical arrows in Fig. 2. The ten candidate spectral lines (identified from the absorption spectrum of Fig. 2) for real-time CH_3SH sensing are listed in column 1 of Table 1. Table 1 shows the calculated candidate CH_3SH line and possible interference in the atmosphere; namely, the first column is the serial number of the candidate spectral line; the second and third columns are the central wavelength and absorbance of the calculated candidate CH_3SH line; the fourth and fifth columns are the central wavelength and absorbance of possible interference; the sixth column is the wavelength space between CH_3SH and its nearby interference. According to the above spectral line selection principle, lines 1, 4, 5, and 10 should be adequate for CH_3SH monitoring because of their strong absorbance and relative isolation from other neighboring interference in the atmosphere. We have selected line 10 (ν_2 C–H symmetric stretch) for CH_3SH monitoring here due to the strongest absorbance and laser availability.

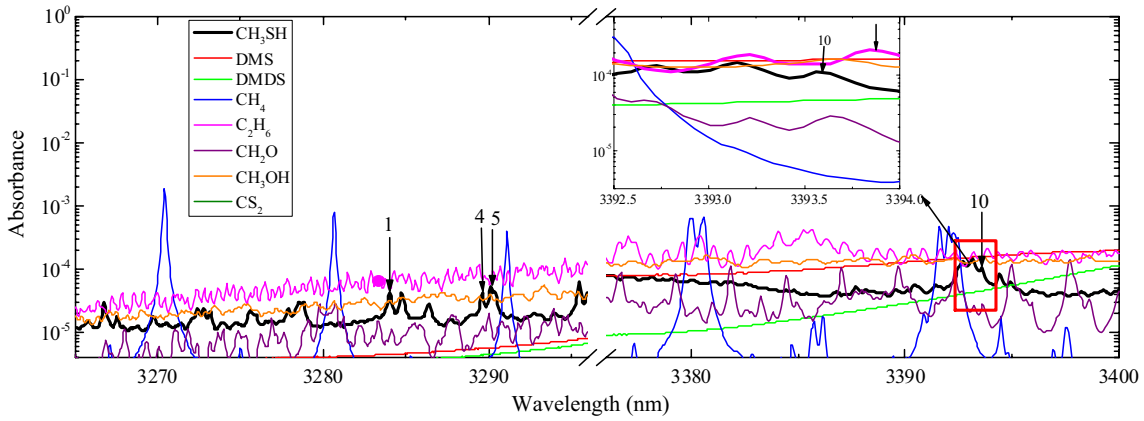

Fig. 3 Spectra of gases typically found in an industrial atmosphere (from the PNNL database). The spectra correspond to 1 ppm × m of each gas, at a temperature of 25 °C

To further examine the specificity of the candidate CH_3SH lines, we screened several molecules with similar structures, including dimethyl sulfide, dimethyl disulfide, carbon disulfide, methane, ethane, formaldehyde, and methyl alcohol. These potentially interfering hydrocarbons should be separated from the CH_3SH absorption band. Figure 3 shows the absorption spectrum of 1-ppm × m CH_3SH in a 1-ppm × m hydrocarbon background from the PNNL database. The spectral region around line 10 (3393.584 nm) has the least interference from these hydrocarbons. Except for ethane, most hydrocarbon backgrounds which have no absorption feature contribute only an offset to the total CH_3SH absorption spectra. However, as shown in the inset of Fig. 3, ethane exhibits appreciable absorption at 3393.863 nm. Its absorbance is a little higher than that of CH_3SH at equal concentrations, but the separation distance is only 0.279 nm. According to the spectral line selection principle, ethane absorption may interfere CH_3SH monitoring. However, the interference can be eliminated using specified algorithms, such as the least squares fitting of a reference line profile, or a multispectral line identification algorithm [30]. Or CH_3SH can be detected without interference only if its concentration is at least two times that of ethane; i.e., the CH_3SH detection threshold increases in the presence of ethane. Except for ethane, Fig. 3 shows that there is virtually no interference from other hydrocarbons at line 10 (3393.584 nm, 2948 cm^{-1}). Thus, it was chosen here as the pilot line for CH_3SH detection.

3 Experimental

The required wavelength range for optimum CH_3SH detection is generated with a single-mode, room-temperature, continuous-wave (CW) DFB-ICL laser (Nanoplus GmbH, Gemany). It is mounted on a TO66 header integrated with a thermoelectric cooler (TEC) and a negative temperature coefficient thermistor, which provides a wide temperature range for laser tuning. Figure 4 shows the laser characteristics. At a chip temperature of 45 °C, the threshold current is 28 mA. With an injection current of 45 mA, it produces 2.4 mW of CW single-mode emission at 3393 nm, and the side-mode suppression ratio is better than 30 dB in single mode.

The tuning characteristics of the DFB-ICL were determined by a FTIR spectrometer (Spectrum GX, Perkin Elmer) with 0.2 cm^{-1} spectral resolution. The current tuning characteristic of the DFB-ICL was obtained by using polynomial fitting, which is $\lambda = 3385.0187 + 0.1186 \times I + 7.29 \times 10^{-4} \times I^2$, while the wavelength tuning via temperature of the DFB-ICL is 0.316 nm/°C. The emission wavelength could be tuned over 3388.60–3393.75 nm by the variation in injection current and chip temperature. Figure 5 shows the tuning characteristics around 3393 nm.

According to the Beer–Lambert law, the sensitivity of TLAS is proportional to the optical path length. Generally, long optical paths are required for highly sensitive measurements, and several multi-pass cells have been developed, such as White cell and Herriott cell. However, alignment stability, long gas exchange time, high cost, and large physical size have limited the use of these multi-pass cells [31]. And the long gas exchange time may prolong the response time of the TLAS system.

We constructed an experimental system with a home-made HWG gas cell, which may greatly improve the response time of the TLAS system for the very small sample volume of only 4 cm^3, as shown in Fig. 6. The gas cell is composed of a HWG (HWEAC10001600, Polymicro) with core diameter of 1 mm and length of 5 m and a home-made coupling component, which couples the mid-infrared laser and the target gas

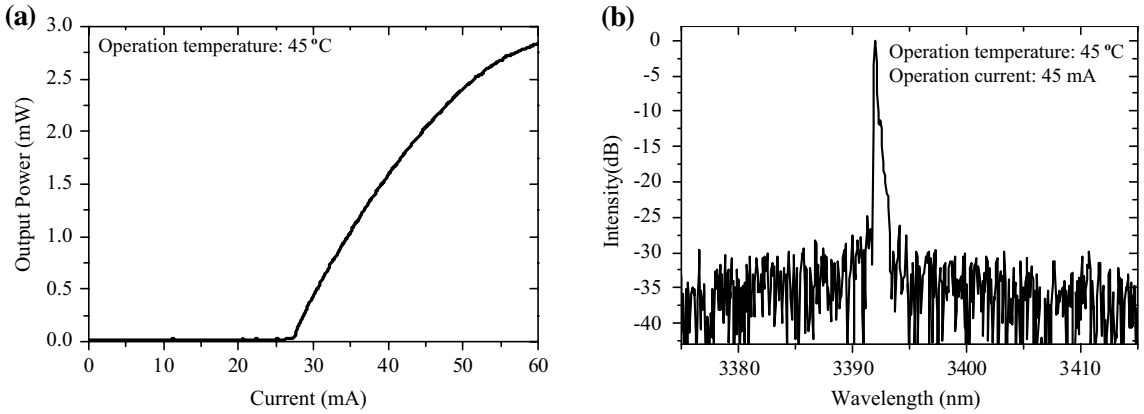

Fig. 4 CW characteristics of the DFB-ICL laser emitting at 3393 nm. **a** Output power versus injection current, **b** emission spectrum (data from Nanoplus GmbH, Gemany)

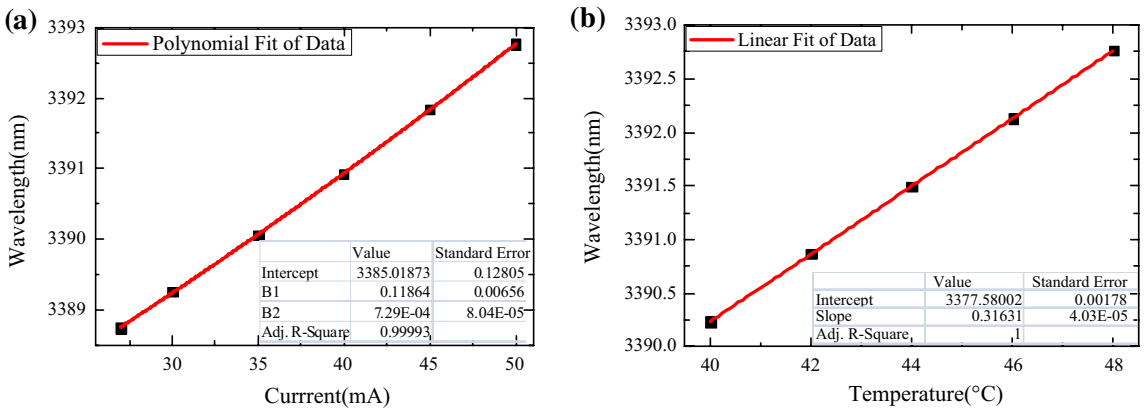

Fig. 5 Tuning characteristics of the DFB-ICL laser, measured with FTIR spectrometer, under injection current (**a**) and temperature (**b**)

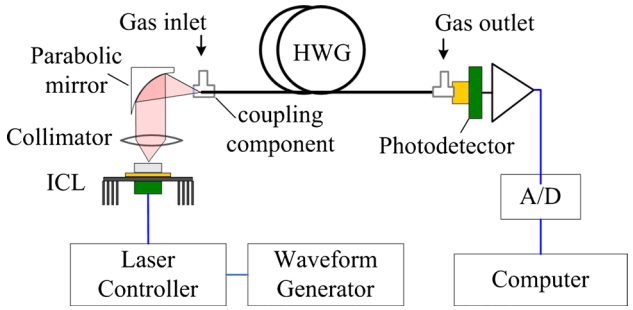

Fig. 6 Schematic of experimental apparatus. HGW: hollow waveguide

to the HWG simultaneously. The mid-infrared laser and the target gas transmit in the same HWG together.

The experimental system comprised with the above-mentioned DFB-ICL laser, the home-made HWG cell, a mid-infrared detector, a laser controller, and a waveform generator. The absorbed and nonabsorbed laser radiation was detected by a photodetector (PDA20H-EC, Thorlabs Inc.) which employs an AC-coupled amplifier with a peak sensitivity of 2.0×10^5 V/W between 1.5 and 4.8 μm.

The laser injection current and the TEC power were supplied by a laser controller (LDC-3908, ILX), while the current modulation (negative ramp at 10 Hz) was supplied by a waveform generator (Fluke 284). The TEC temperature was kept constant during measurements; thus, wavelength tuning was realized via direct modulation of the injection current. Data were acquired using LabVIEW software (National Instruments).

4 Results

The CH_3SH absorption region around 3393.5 nm was achieved by using a laser temperature of 49.5 °C and an injection current that was swept from 35 to 55 mA at 10 Hz.

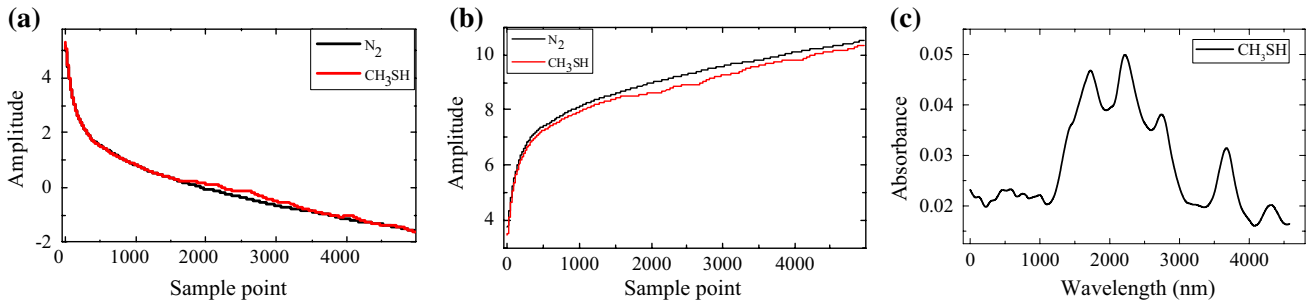

Fig. 7 **a** Detected raw spectral signal of N_2 and CH_3SH, **b** the corrected signal of **a,** and **c** the absorbance of CH_3SH

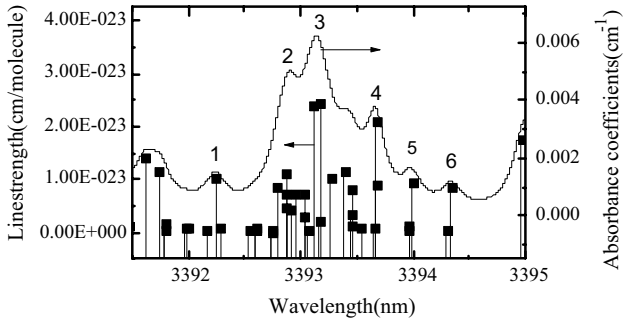

Fig. 8 Absorption coefficients and line strength of C_2H_4 from the HITRAN database

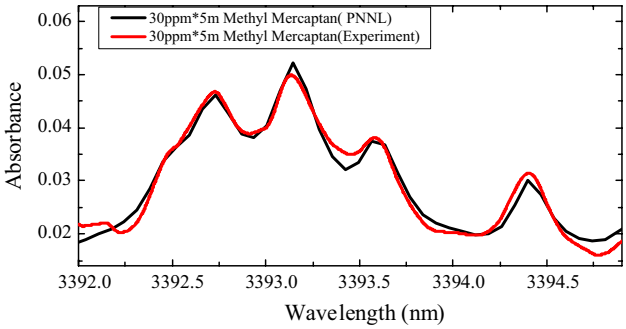

Fig. 9 Tunable laser direct absorption by CH_3SH compared with an absorption spectrum from the PNNL database

The detected analog spectral signals converted into digital signals in order to be processed by computer. The sample rate is set as 50 kilo-samples per second (kSPS). The detected raw signal of N_2 and CH_3SH is shown in Fig. 7a. The phase correction of the recorded signal was performed by inversing the raw signal and adding an offset, and the offset is determined by fitting the emitting characteristics of the laser descript in Fig. 4a. Figure 7b shows the corrected spectral signal of Fig. 7a. We subtracted the N_2 background signal from the CH_3SH TLAS direct absorption signal and obtained the CH_3SH TLAS direct absorption spectrum according to the Beer–Lambert law, shown in Fig. 7c.

Then, the laser emission wavelength was calibrated by using several 1 % ethylene (C_2H_4) absorption lines as wavelength markers. We got the C_2H_4 spectral lines during the 3391.5–3395 nm wavelength range from the HITRAN database. Figure 8 shows absorption coefficients and line strength of C_2H_4 from the HITRAN database.

We use the same parameters and the same method to get the C_2H_4 TLAS direct absorption spectrum. Then, we got the C_2H_4 spectral lines from the experimental result during the 3391.5–3395 nm wavelength range. The wavelength of C_2H_4 absorption from the HITRAN database and sample point of C_2H_4 absorption from the experimental result are fitted by a second-order polynomial. The fitting result is the Eq. (3):

$$\lambda = 3391.09 + 7.2\text{E-}4 \times N + 2.26E - 8 \times N^2 \quad (3)$$

Finally, we compared the CH_3SH TLAS direct absorption spectrum obtained from the TLAS experiment with the absorption spectrum from the PNNL database. Both the absorption spectrum of 30 ppm × 5 m CH_3SH from the PNNL database (black curve) and the direct absorption of 30 ppm CH_3SH reference gas (red curve) measured by TLAS system are plotted in Fig. 9. There is an excellent agreement between the CH_3SH TLAS spectrum and the FTIR spectrum from the PNNL database.

TLAS linearity was investigated for CH_3SH concentrations from 3 to 30 ppm, in 3-ppm steps, made with a gas mixer (MODEL 821, Signal Instrument), and diluted with dry nitrogen. However, the detector receiving the spectral signal contained an AC coupling amplifier, so the spectra for the different concentrations should have different background spectra. To determine an accurate CH_3SH concentration, each CH_3SH spectrum was implemented by Savitzky–Golay smoothing with three order of the polynomial function to get the background spectrum of each CH_3SH spectrum; then, the background spectrum was subtracted from the corresponding measured CH_3SH spectrum and finally got the resulting fast-change signals. For example, Fig. 10 shows the background signal and CH_3SH direct

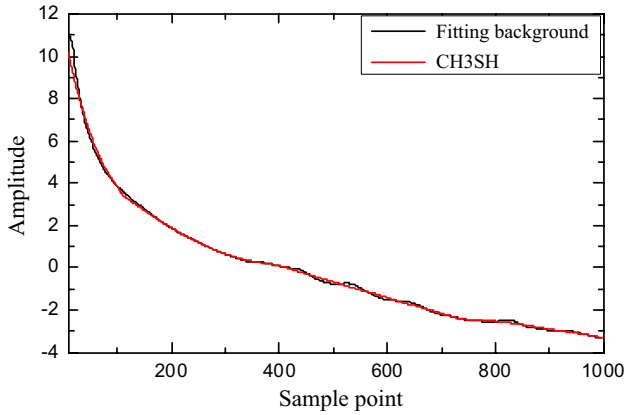

Fig. 10 Background signal and CH_3SH direct absorption signal

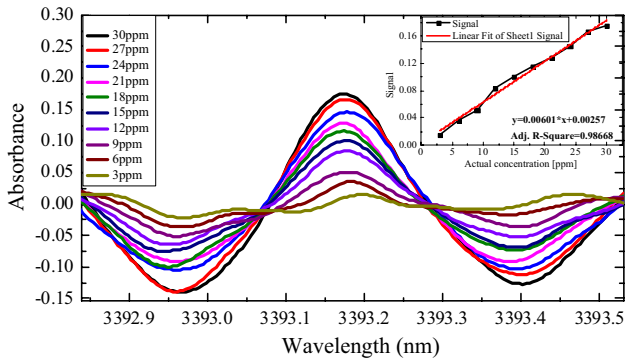

Fig. 11 Direct absorption signal from a series of calibrated CH_3SH gas mixtures from 3 to 30 ppm, with an inset of measured versus actual concentrations from 3 to 30 ppm

absorption signal, which referred to the processing algorithms of differential optical absorption spectroscopy. The resulting fast-change signals from 3392.8 to 3393.5 nm corresponding to the CH_3SH absorption feature for a set of calibrated gas mixtures are shown in Fig. 11. The inset is the measured versus actual CH_3SH concentration for 3–30 ppm. The results demonstrate that simple CH_3SH sensing over a fairly wide range of concentrations can be obtained using the Beer–Lambert law.

To test the stability and response time of the measurements, we performed the Allan variance $\sigma_A^2(\tau)$ to assess the CH_3SH flow measurements. It was first introduced by Allan in 1966 for characterization of frequency standards and then applied to TLAS by Werle et al. [32] to assess the time stability of a measurement or a measurement system [23]. Each data point analyzed by Allan variance in Fig. 12 was obtained by a curve fit to real-time CH_3SH absorption spectra at the 10 Hz scan rate. The Allan variances are for a 5-m path length, expressed in units of $(ppbv)^2$. The best detection limit under constant room-temperature conditions

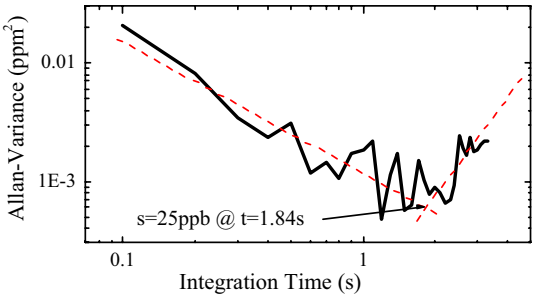

Fig. 12 Measurement of a 30-ppm CH_3SH calibration gas mixture, with the corresponding "Allan Plot" as a function of integration time. The minimum indicates that the most sensitive measurements can be achieved with a 1.84 s integration time, yielding a minimum of 25 ppbv × 5 m

was 25 ppbv × 5 m, or 125 ppbv × m, for an integration time of 1.84 s. We concluded from the result of Allan variance the system drift starts from 1.84 s, because the experimental setup was not a mature instrument, and the experiment parameters were not optimized sufficiently. This limit, however, is not applicable for longer periods of time because drift starts to dominate.

5 Conclusion

We have demonstrated detection of CH_3SH in the wavelength region around 3392 nm using a room-temperature DFB-ICL. The CH_3SH absorption bands (ν_2) in the 3260–3400 nm region are the strongest IR bands and avoid interference from industrial pollution. We characterize absorption features of calibrated CH_3SH spectra under laboratory conditions. We demonstrate that the characteristics of a room-temperature DFB-ICL make it suitable for CH_3SH TLAS measurements. In addition, higher sensitivity is achieved by using a 5-m HWG gas cell. The best detection limit at room temperature is 125 ppbv × m with an integration time of 1.84 s, corresponding to an absorbance of 1.34×10^{-4} (near the theoretical detection limit). In conclusion, the TLAS system is a feasible method for real-time monitoring of CH_3SH in industrial environments.

Acknowledgments This work is supported by the Special-funded Program on National Key Scientific Instruments and Equipment Development (2012YQ06016501) of China and the National Natural Science Foundation of China (Grant No. 61505142) and Natural Science Foundation of Hebei Province (Grant No. F2014202065).

References

1. B.P. Lomans, C. van der Drift, A. Pol, H.J.M. Op den Camp, Cell. Mol. Life Sci. **59**, 575 (2002)

2. R. Pal, K.-H. Kim, E.-C. Jeon, S.-K. Song, Z.-H. Shon, S.-Y. Park, K.-H. Lee, S.-J. Hwang, J.-M. Oh, Y.-S. Koo, Environ. Monit. Access. **148**, 109 (2009)
3. K.-H. Kim, Atmos. Environ. **40**, 6567 (2006)
4. J. Lin, J. Aoll, Y. Niclass, M.I. Velasco, L. Wünsche, J. Pika, C. Starkenmann, Environ. Sci. Technol. **47**, 7876 (2013)
5. A. Feilberg, D. Liu, A.P.S. Adamsen, M.J. Hansen, K.E.N. Jonassen, Environ. Sci. Technol. **44**, 5894 (2010)
6. J.E. Amoore, E. Hautala, J. Appl. Toxicol. **3**, 272 (1983)
7. S. Jayaraman, R. Walia, N. Alagirisamy, Sensor. Actuat. B **148**, 54 (2010)
8. S. Vance, L.E. Christensen, C.R. Webster, K. Sung, Planet. Space Sci. **59**, 299 (2011)
9. K. Toda, H. Kuwahara, H. Kajiwara, K. Hirota, S.-I. Ohira, Anal. Chim. Acta **841**, 1 (2014)
10. D.J. Paetznick, G.A. Reineccius, T.L. Peppard, J.M. Herkert, P. Lenton, J. Breath Res. **4**, 017106 (2010)
11. L.J.J. Catalan, V. Liang, C.Q. Jia, J. Chromatogr. A **1136**, 89 (2006)
12. A. Tangerman, E.G. Winkel, J. Breath Res. **2**, 017010 (2008)
13. N. Tanda, J. Washio, K. Ikawa, K. Suzuki, T. Koseki, M. Iwakurac, J. Dent. **35**, 552 (2007)
14. M. Mori, Y. Itagaki, Y. Sadaoka, S.-I. Nakagawa, M. Kida, T. Kojima, Sensor. Actuat. B **191**, 351 (2014)
15. A. Yamaguchi, K. Masunaga, K. Hayashi, K. Toko, IEEJ Trans. Electr. Electr. **4**, 372 (2009)
16. Z.H. Li, S.G. Sun, J.L. Marty, Sensor Actuat. B Chem. **192**, 680 (2014)
17. K. Mitsubayashi, T. Minamide, K. Otsuka, H. Kudo, H. Saito, Anal. Chim. Acta **573**, 75 (2006)
18. T. Minamide, K. Mitsubayashi, H. Saito, Sensor. Actuat. B **108**, 639 (2005)
19. Y. Tanaka, T. Nakamoto, T. Moriizumi, Sensor. Actuat. B **119**, 84 (2006)
20. M.W. Sigrist, R. Bartlome, D. Marinov, J.M. Rey, D.E. Vogler, H. Wachter, Appl. Phys. B **90**, 289 (2008)
21. P. Kluczynski, S. Lundqvist, S. Belahsene, Y. Rouillard, L. Nähle, M. Fischer, J. Koeth, Appl. Phys. B **108**, 183 (2012)
22. P. Kluczynski, M. Jahjah, L. Nähle, O. Axner, S. Belahsene, M. Fischer, J. Koeth, Y. Rouillard, J. Westberg, A. Vicet, S. Lundqvis, Appl. Phys. B **105**, 427 (2011)
23. P. Kluczynski, S. Lundqvist, S. Belahsene, Y. Rouillard, Opt. Lett. **34**, 3767 (2009)
24. S. Lundqvist, P. Kluczynski, R. Weih, M.V. Edlinger, L. Nähle, M. Fischer, A. Bauer, S. Höfling, J. Koeth, Appl. Opt. **51**, 6009 (2012)
25. M. Horstjan, Y.A. Bakhirk, A.A. Kostere, R.F. Curl, F.K. Tittel, C.M. Wong, C.J. Hill, R.Q. Yang, Appl. Phys. B **79**, 799 (2004)
26. K. Krzempek, R. Lewicki, L. Nähle, M. Fischer, J. Koeth, S. Belahsene, Y. Rouillard, L. Worschech, F.K. Tittel, Appl. Phys. B **106**, 251 (2012)
27. S.W. Sharpe, T.J. Johnson, R.L. Sams, P.M. Chu, G.C. Rhoderick, P.A. Johnson, Appl. Spectrosc. **58**, 1452 (2004)
28. L.S. Rothman, I.E. Gordon et al., J. Quant. Spectrosc. RA. **130**, 4 (2013)
29. X. Zhou, X. Liu, J.B. Jeffries, R.K. Hanson, Meas. Sci. Technol. **14**, 1459 (2003)
30. C.S. Goldenstein, C.L. Strand, I.A. Schultz, Appl. Opt. **53**, 356 (2014)
31. G.J. Fetzer, A.S. Pittner, W.L. Ryder, D.A. Brown, Appl. Opt. **41**, 3613 (2001)
32. P. Werle, R. Miicke, F. Slemr, Appl. Phys. B **57**, 131 (1993)